Multimodal profiling reveals tissue-directed signatures of human immune cells altered with age

Steven B. Wells[1,2*], Daniel B. Rainbow[3*], Michal Mark[4*], Peter A. Szabo[2*], Can Ergen[5*], Ana Raquel Maceiras[6*], Daniel P. Caron[2], Elior Rahmani[5], Eli Benuck[4] ,Valeh Valiollah Pour Amiri[5], David Chen[1], Allon Wagner[5], Sarah K. Howlett[3], Lorna B. Jarvis[3], Karen L. Ellis[3], Masaru Kubota[7], Rei Matsumoto[7], Krishnaa Mahbubani[8], Kouresh Saeb-Parsy[8], Cecilia Dominguez-Conde[6], Laura Richardson[6], Chuan Xu[6], Shuang Li[6], Lira Mamanova[6], Liam Bolt[6], Alicja Wilk[6], Sarah A. Teichmann[6,9ǂ], Donna L. Farber[2,7ǂ], Peter A. Sims[1,10ǂ], Joanne L. Jones[3ǂ], Nir Yosef[4,5ǂ]

[1] Department of Systems Biology, Columbia University Irving Medical Center, New York, NY

[2] Department of Microbiology and Immunology, Columbia University Irving Medical Center, New York, NY

[3] Department of Clinical Neurosciences, University of Cambridge, Cambridge, UK

[4] Department of Systems Immunology, Weizmann institute, Rehovot, Israel

[5] Department of Electrical Engineering and Computer Science and Center for Computational Biology, University of California, Berkeley, CA

[6] Wellcome Sanger Institute, Wellcome Genome Campus, Hinxton, Cambridge, UK.

[7] Department of Surgery, Columbia University Irving Medical Center, New York, NY

[8] Department of Surgery, University of Cambridge, Cambridge, UK

[9] Theory of Condensed Matter, Cavendish Laboratory, University of Cambridge, Cambridge, UK

[10] Department of Biochemistry & Molecular Biophysics, Columbia University Irving Medical Center, New York, NY

* Equal contribution

ǂ Equal contribution

Correspondence: nir.yosef@weizmann.ac.il, df2396@cumc.columbia.edu pas2182@cumc.columbia.edu, jls53@medschl.cam.ac.uk, st9@sanger.ac.uk

Keywords: Single cell genomics, Lymphocytes, myeloid cells, macrophages, tissue residence, mucosal immunity, immune senescence, aging, tissue atlas, counterfactual analysis

ABSTRACT

The immune system comprises multiple cell lineages and heterogeneous subsets found in blood and tissues throughout the body. While human immune responses differ between sites and over age, the underlying sources of variation remain unclear as most studies are limited to peripheral blood. Here, we took a systems approach to comprehensively profile RNA and surface protein expression of over 1.25 million immune cells isolated from blood, lymphoid organs, and mucosal tissues of 24 organ donors aged 20-75 years. We applied a multimodal classifier to annotate the major immune cell lineages (T cells, B cells, innate lymphoid cells, and myeloid cells) and their corresponding subsets across the body, leveraging probabilistic modeling to define bases for immune variations across donors, tissue, and age. We identified dominant tissue-specific effects on immune cell composition and function across lineages for lymphoid sites, intestines, and blood-rich tissues. Age-associated effects were intrinsic to both lineage and site as manifested by macrophages in mucosal sites, B cells in lymphoid organs, and T and NK cells in blood-rich sites. Our results reveal tissue-specific signatures of immune homeostasis throughout the body and across different ages. This information provides a basis for defining the transcriptional underpinnings of immune variation and potential associations with disease-associated immune pathologies across the human lifespan.

Abbreviations: BLO, Blood; BMA Bone Marrow; SPL, Spleen; LN, Lymph Node; LNG, Lung; JEJ, Jejunum. TN, naive T cell; TCM, central memory T cell; TEM, effector-memory T cell; TEMRA, terminal effector cell; TRM, Tissue resident memory T cell; TREG, regulatory T cell.

INTRODUCTION

The immune system comprises a complex network of specialized cells in diverse tissue sites to protect against infections and cancer, regulate inflammation, and resolve tissue damage or injury. In humans, there is tremendous heterogeneity in immune responses across tissues and over age, yet the underlying mechanisms remain difficult to ascertain.

Myeloid lineage cells, such as macrophages, monocytes, and dendritic cells, play a crucial role in coordinating innate immunity by managing inflammatory responses and antigen processing directly in tissue sites of pathogen encounter such as lungs, intestines, skin and other sites. The subsequent induction of adaptive immunity involves the activation of antigen-specific T and B lymphocytes in lymphoid organs thereby promoting B cell differentiation to antibody secreting cells, and T cell differentiation to effector cells, which migrate to infection sites for pathogen clearance. Immune memory develops from activated lymphocytes and persists as non-circulating, tissue resident memory T cells (TRM) [1], memory B cells in both lymphoid and mucosal sites, and circulating memory populations across sites.

However, the identity and heterogeneity of human immune cells across lineages, tissues, and age remain poorly understood, as most studies of human immunity are confined to the sampling of peripheral blood [2] or to multi-tissue analysis of restricted cohorts [3]. Recent advances in single-cell technologies for transcriptome profiling have enabled comprehensive identification of individual cell types, their function, and heterogeneity in tissues throughout the body. Cellular atlases specific to organs such as lungs [4], liver [5], brain [6], and reproductive tract [7] provide comprehensive datasets for elucidating developmental pathways and serve as new baselines for understanding tissue-specific disease states.

For immune cells, investigating many tissues across diverse ages is necessary to encompass the entire breadth of the immune system and identify sources of variation [8]. We have pioneered the study of human immune cells across diverse anatomic sites using tissues obtained from organ donors, enabling phenotypic, functional, and single cell profiling of immune cells from multiple tissues within and between individuals [9–13]. Our studies of lymphocytes revealed that T and NK cell subset composition, tissue residence, and functional attributes are specific to the tissue [9,12,14–16], suggesting that tissue may play a dominant role in immune cell states across lineages and their variation with age.

In this study, we sought to define the role of tissue and age in immune cell identity and function, accounting for all major immune lineages. We used cellular indexing of transcriptomes and epitopes (CITE-seq) to

simultaneously profile transcriptome and surface marker expression of myeloid and lymphoid-lineage cells in 14 tissue sites of 24 organ donors, aged 20-75 years. Through multimodal classification, probabilistic modeling, and various comparative analyses, we reveal how certain lineages and subsets exhibit tissue-specific adaptations, and how aging affects the cellular and molecular composition of immune lineages across and within tissues.

RESULTS

Multimodal profiling and classification of immune lineages across sites and ages

We isolated mononuclear cells from blood, lymphoid organs, lungs, airways, intestines, and other sites, using well-established protocols (see Methods)[12,13] (**Fig. 1A, B**). We performed scRNA-seq on 24 donors using the 10x Genomics platform, of whom 22 had CITE-seq–profiling with at least 130 proteins (see Methods, **Supplementary Table 1**). The organ donors originated from New York City (US) and Cambridge, England (UK), and were free of chronic infection, cancer, and overt disease (**Supplementary Table 2**). After stringent quality control, we obtained 1.27 million immune cell events from 14 tissue sites. This included ten key sites, each with at least 75,000 cells, including blood (BLO), bone marrow (BMA) spleen (SPL), lungs (LNG) which include bronchoalveolar lavage (BAL) and lung parenchyma (PAR), lymph nodes (LN) including lung-associated (LLN), mesenteric (MLN), and iliac (ILN), and jejunum (JEJ) divided into the jejunal intraepithelial layer (JEL), and jejunal lamina propria (JLP), and these sites were subsequently analyzed as described below (**Fig. 1B**). When available, immune cells were also purified from liver (LIV), skin (SKN), colon epithelium (CEL) and lamina propria (CLP). While these data will be made available as part of our annotated dataset, they, along with polymorphonuclear cells (mast cells and neutrophils), were not included in subsequent analyses due to low cell and donor numbers **(Extended data Fig. 1A**).

To integrate data from the ten key tissue sites and 24 donors we leveraged multi-resolution variational inference (MrVI). Designed particularly for cohort studies, MrVI provides two levels of integration: one that primarily reflects variation between cell states (allowing for unified annotation of cell states in all samples) and another accounting for differences between samples (allowing for comparative analysis) [17]. The integrated dataset was visualized using uniform manifold approximant and projection (UMAP) [18], showing similar results across US and UK donors (**Fig. 1C, Extended data Fig. 1**). When visualized by tissue of origin, immune cells from blood, BMA, and LN integrated similarly, while cells from lungs, jejunum, and to a lesser extent, spleen

localized by tissue (**Fig. 1D**). For immune cell subset annotation, we used the MMoCHi (MultiModal Classifier Hierarchy) algorithm [19] that leverages both gene and cell surface protein expression to hierarchically classify cells into predefined categories (**Supplementary Fig 1, Supplementary Tables 3, 4**). MMoCHi identified six major immune cell lineages: T lymphocytes, innate lymphocytes, B lymphocytes, myeloid cells, mast cells, and progenitors, each of which clustered distinctly and exhibited various levels of integration by tissue (**Fig. 1D,E**).

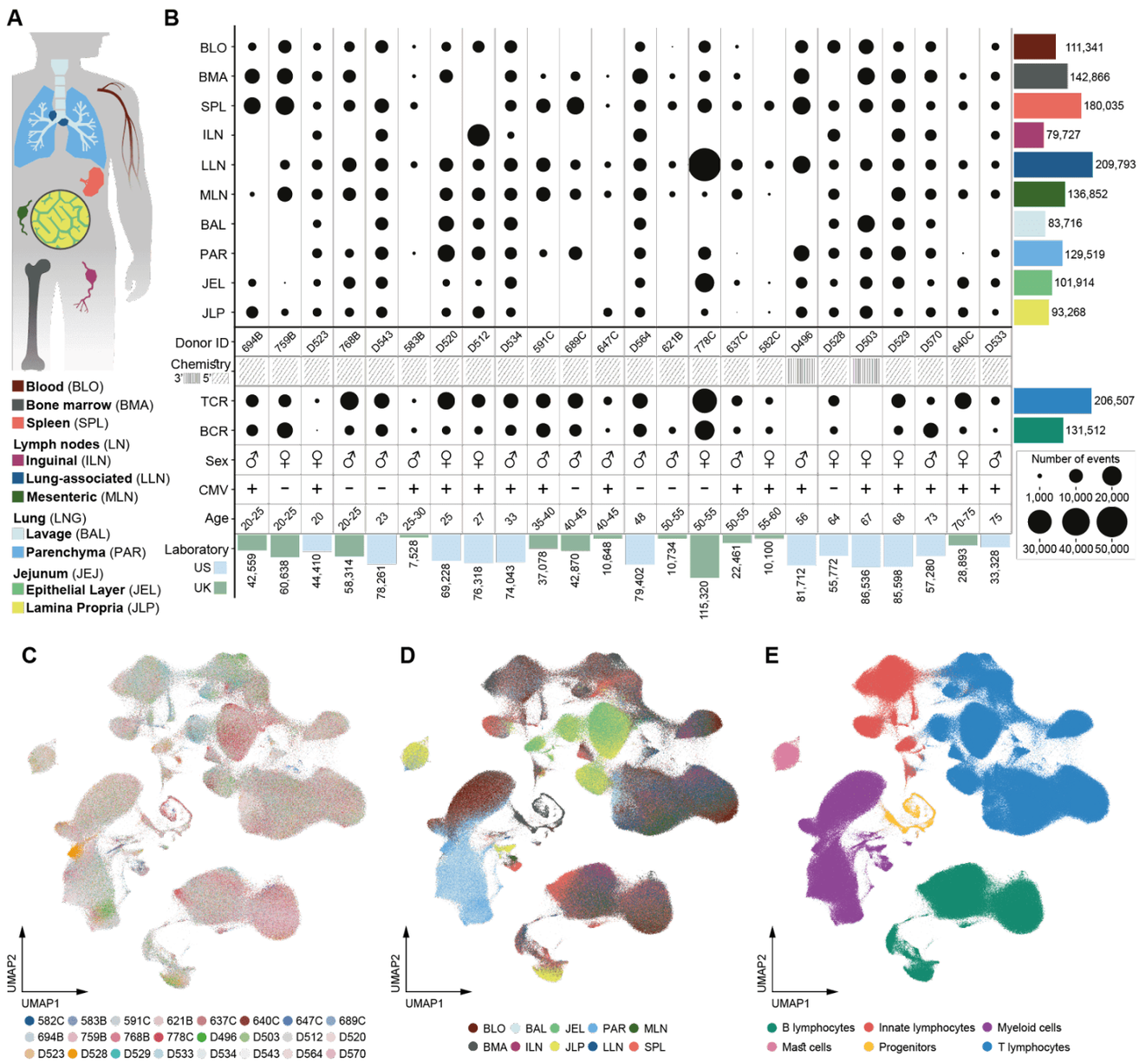

<u>Figure 1. A multi-lineage human immune cell atlas across tissues and age.</u> **(A)** Schematic of ten tissue sites used in analysis. **(B)** Dotplot of cells by donor and tissue site showing for each donor the sequencing chemistry, sex, CMV status, age, and whether the respective samples were obtained and processed in NY or UK. The scRNAseq data from 1,269,031 events are visualized as UMAP embeddings colored by donor. Bars in the bottom of the panels depict the overall number of cells profiled from each donor. Bars on the right of the panels depict the overall number of cells in each tissue across all donors. **(C)**, by tissue site **(D)**,or by major lineage as determined by the MMoCHi classifier **(E)**.

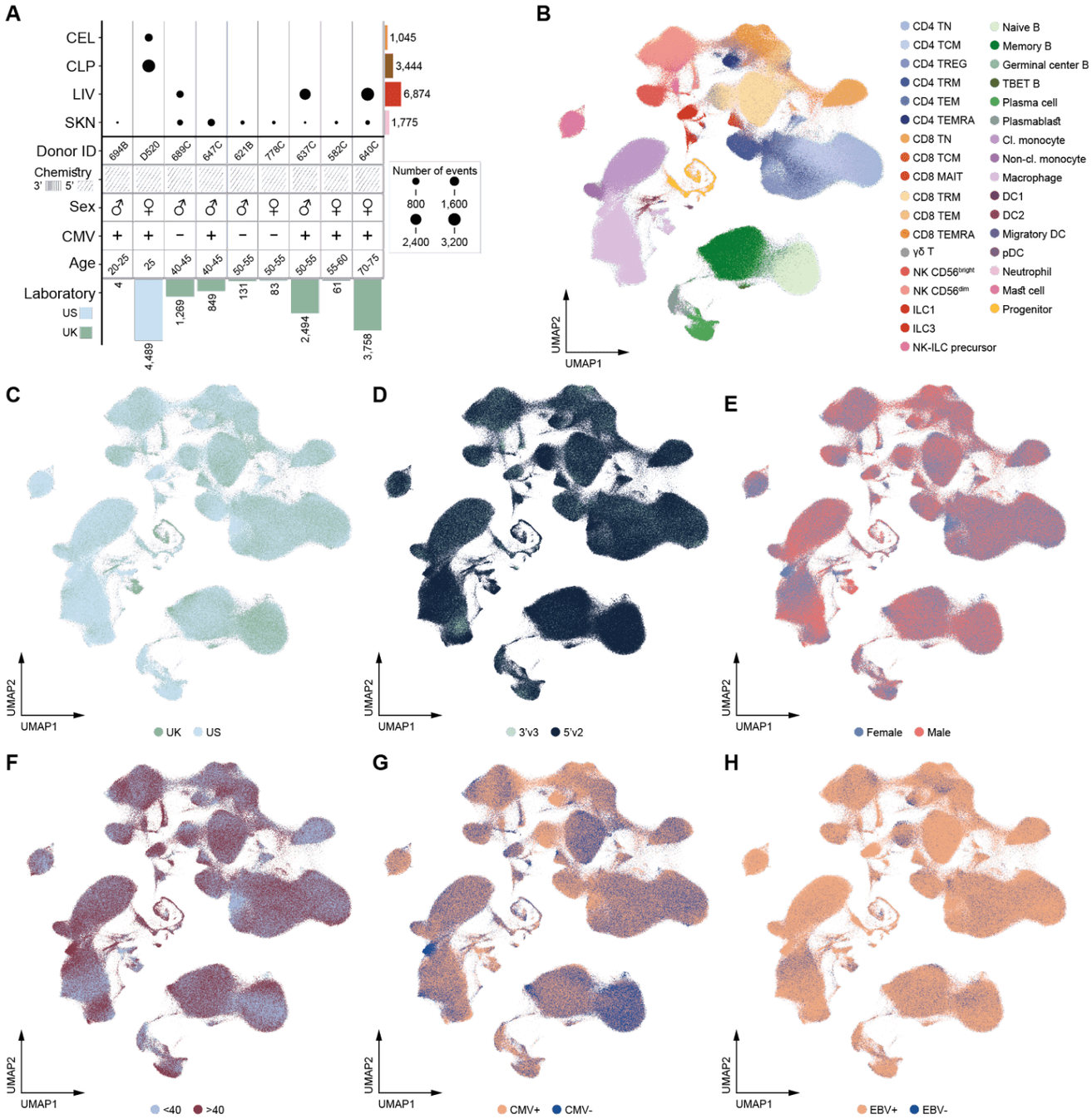

Extended data Figure 1: Tissue sites excluded from study and UMAPs of covariates. **(A)** Schematic of four tissue sites collected yet excluded from analysis. **(B)** UMAP of MMoCHi cell annotations. **(C, D, E, F, G, H)** UMAPs colored by collecting laboratory, 10x chemistry, sex, age groups, CMV status, and EBV status.

Using MMoCHi , we further defined thirteen T cell subsets, five NK/ILC subsets, six B cell subsets and seven myeloid subsets (**Fig. 2**). Manual curation was also performed for greater depth of annotation, resulting in 74 cell types and states (**Extended data Fig. 2, Supplementary Fig. 2**). The T cell compartment (610,429 cells) was classified into relatively rare γδ T cells, which develop early in ontogeny, and predominant αβ T cells consisting of $CD4^+$ and $CD8^+$ lineages subdivided into naïve, terminal effector (TEMRA), and memory – effector-memory (TEM), central memory (TCM), and tissue resident memory (TRM) – subsets, along with $CD4^+$ regulatory T cells (Treg) defined based on surface markers and lineage defining genes [16,20,21] (**Fig. 2A, B**). Surface markers were used to enable the identification of T cell subsets that were not readily resolved by scRNA-seq alone[11,12]. For example, CD45RA surface expression was used to distinguish naive ($CD45RA^+$) from TCM ($CD45RA^-$), as each exhibit lymphoid homing profiles (CD62L, *CCR7*), and TEM ($CD45RA^-$) from TEMRA ($CD45RA^+$) cells, as both have effector-like profiles. In addition, TRM were distinguished from the TEM subset based on surface expression of core markers CD69, CD103, and CD49a [16] (**Supplementary Table 3**). TEM and TEMRA populations could be further subdivided into functional subsets based on expression of genes encoding cytolytic mediators (*GZMB*, *GZMK*) and the cytokine IL-17 (**Extended data Fig. 2** and **Supplementary Fig. 2**).

When visualized by tissue, naïve and TCM subsets were distributed in blood, BMA and lymphoid organs, TRM were predominant in the jejunum and found in lung and LN, and Treg were enriched in LN (**Fig. 2B**), consistent with previous flow cytometry analysis [9,12,22]. Mucosal-associated invariant T (MAIT) cells distinguished by TCR expression, CD161 and other markers[23] were enriched in spleen, BMA, and LNG (**Fig. 2A,B**). T cell receptor (TCR) clonal analysis provided additional correlative evidence for T cell subset delineation and tissue distribution (**Supplementary Fig. 3**). In particular, $CD8^+$ T cells exhibited greater clonal expansion compared to $CD4^+$ T cells, the TEMRA subset had the highest clonality across sites followed by TEM cells, and tissues with predominant memory T cells had the highest clonality compared to LN which contain naive populations with high diversity (**Supplementary Fig. 3**). These findings were consistent with previous TCR analysis of tissue subsets [12,24].

Innate lymphocytes (130,414 cells) across tissues consisted mainly of the $CD56^{dim}$ mature NK subset, characterized by surface expression of CD16 and genes associated with cytolytic function (*KLRF1*, *GZMB*), along with the less abundant $CD56^{bright}$ (immature) NK cells with lower CD16 expression (**Fig. 2C,D**). Innate lymphoid cells (ILC) including ILC1 ($CD16^-$*NCR2*$^+$*IL7R*$^-$) and ILC3 (*IL7R*$^+$*KIT*$^+$*RORC*$^+$)[25] subsets were also detected, but at lower frequencies (**Fig. 2C,D**). Across tissues, $CD56^{dim}$ cells were present mostly in blood,

149 BMA, spleen, and lungs, while CD56^{bright} cells were found in most tissues and enriched in the spleen (**Fig.**
150 **2C,D)**. ILC1, which expressed high levels of the tissue residency markers CD69, CD49a and CD103, were
151 found predominantly in the jejunum, while ILC3s were mainly in LN, spleen, and mucosal sites (**Fig. 2C,D**).
152 Putative NK-ILC precursors, resembling both CD56^{bright} NK and ILC3s (CD127^{+}CD44^{+}*GPR183*$^{+}$) were found
153 mainly in blood, BMA, lung and spleen (**Fig. 2C,D** and **Supplementary Fig. 2**), while a population with
154 characteristics of ILC1 and ILC3 (ILC1-3 "Transitional", *NCR2*$^{+}$CD127^{+}) was exclusive to jejunum (**Extended**
155 **data Fig. 2** and **Supplementary Fig. 2**)

156 The B cell compartment (272,162 cells) (**Fig. 2E,F**) was classified into six major subsets including: naive B
157 cells (IgD^{+}), memory B cells (CD27^{+}), germinal center (GC) B cells that express *AICDA* (activation-induced
158 adenosine deaminase (AID) for immunoglobulin class switch recombination [26]), plasma cells that express *SDC1*
159 (CD138) and highly express immunoglobulin genes, and plasmablasts that express proliferation-associated
160 genes (*MKI67*, *TOP2A*). A subset of "Atypical B cells" (CD27^{-}IgD^{-}) which express *TBX21* encoding the
161 transcription factor T-BET [27,28] was identified at low frequencies across multiple sites (**Fig. 2E,F, Extended**
162 **data Fig. 2**). Manual annotation revealed an additional low frequency population of pro-B cells expressing
163 *MME*, *SOX4* and CD38 restricted to the bone marrow (**Extended data Fig. 2** and **Supplementary Fig. 2**).
164 Overall, B cells were found mostly in lymphoid organs and blood; naïve B cells were in blood, spleen, and LN,
165 and memory B cells were predominantly distributed in spleen and LN. A proportion of these lymphoid memory
166 B cells expressed CD69, denoting tissue resident B cells [29]. Plasma cells were enriched in the jejunum lamina
167 propria while plasmablasts were enriched in lymphoid organs (**Fig. 2E,F**). B cell receptor (BCR) analysis
168 provided additional confirmation and insights into subsets and tissue distribution; plasmablasts exhibited the
169 highest clonal expansion across lymphoid sites, while memory B and plasma (but not naive) cells expressed
170 mutated BCR (**Supplementary Fig. 4A-G**). Across sites, jejunum was enriched with plasma cells expressing
171 IgA, while blood contained fewer memory B cells and lower mutation frequencies compared to all tissues
172 examined (**Supplementary Fig. 4H-J**)

173 Myeloid-lineage cells (225,268 cells) comprised of macrophages, classical and non-classical monocytes,
174 and dendritic cell (DC) subsets, including DC1 (*CLEC9A*$^{+}$), DC2 (*CLEC10A*$^{+}$), migratory DC (*CCR7*$^{+}$), and
175 Plasmacytoid DC (pDC; CD123^{+}*LILRA4*$^{+}$) (**Fig. 2G,H**). Classical monocytes were enriched mostly in blood
176 while non-classical monocytes were also found in BMA and lung. pDCs were enriched in the bone marrow,
177 while other DC subsets were found in the lung, jejunum, and LN (**Fig. 2G,H**). Macrophages were found
178 predominantly in the lungs, but were also present at low frequencies in the jejunum, spleen, and LN (**Fig. 2H,**

Extended data Fig. 2). By manual annotation, macrophages are further subdivided, into *MARCO*$^{+}$ macrophages enriched in the lung, *SPIC*$^{+}$ macrophages enriched in the spleen and *SDS*$^{+}$ macrophages that are found predominantly in the jejunum (**Extended data Fig. 2** and **Supplementary Fig. 2**). Collectively, this comprehensive annotated map of immune cells across major lineages and tissues using multimodal profiling can serve as a reference for annotations, embeddings, and other types analyzes to enable future studies; e.g., using pre-trained models in the popV framework [30] (**Supplementary Fig. 5**).

Collating all of the lineage and subset annotations within and across tissues reveals tissue-specific immune cell compositions with some lineages showing varying proportions between donors (**Fig. 2I, Extended data Fig. 2, Supplementary Fig. 6**). Blood, BMA and spleen contain a similar complement of immune cell subsets with some site specific differences; BMA contained fewer naïve T cells, additional memory T cell subsets, more NK cells and fewer monocytes relative to blood, while spleen contained more memory B cells, NK cell subsets, and lower monocyte proportions compared to blood. Moreover, LN contained increased naïve, TCM, TRM, memory B cells, and macrophages and fewer monocytes compared to spleen and BMA. Lungs and jejunum were most distinct from lymphoid organs and each other; lung contained the greatest proportion of macrophages, low frequencies of B cells and multiple memory T cell subsets, while intestines contained largely TRM populations, ILC1, macrophages and low frequencies of B cells. These analyses reveal a tissue intrinsic nature of immune cell composition for all immune cell lineages.

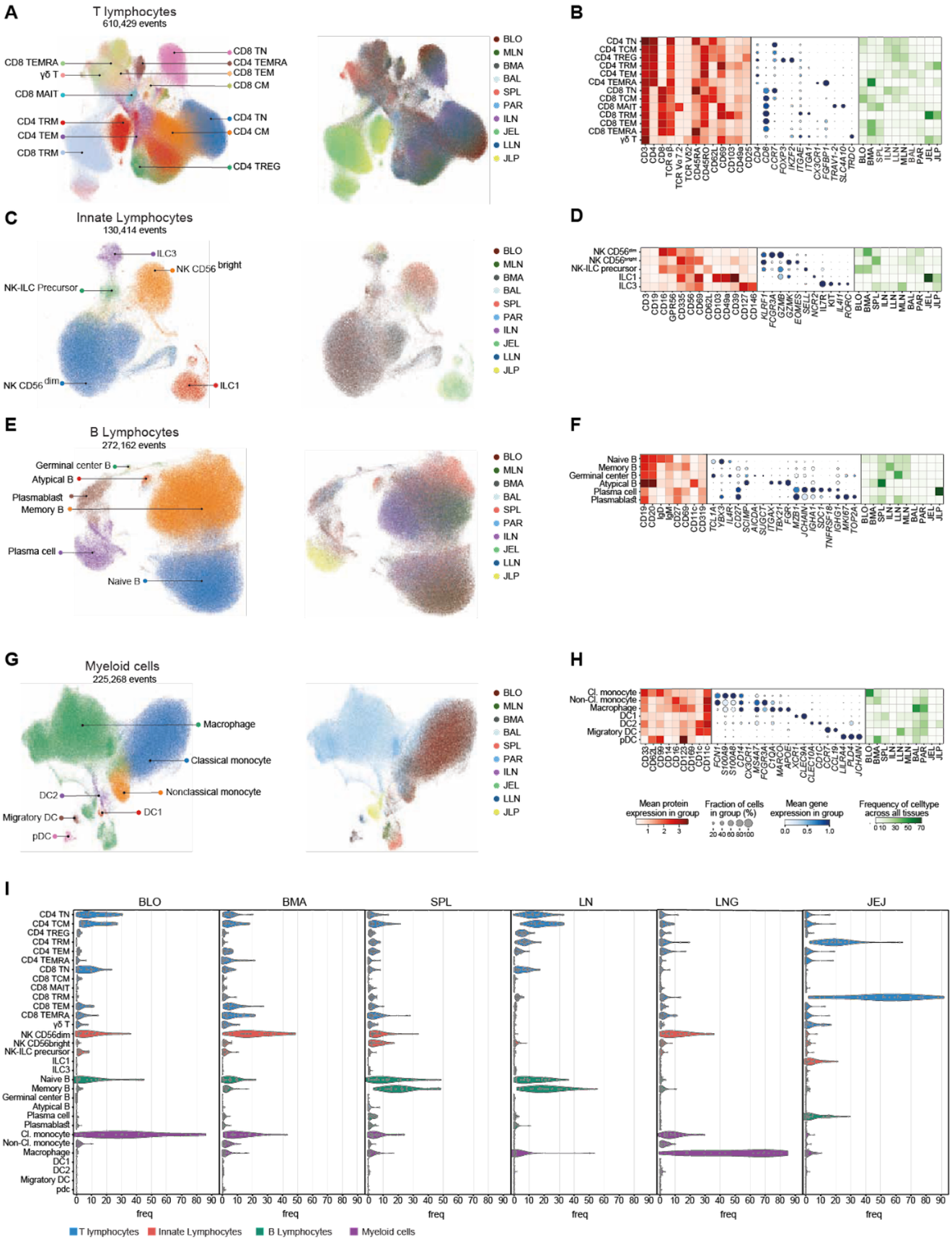

Figure 2: Heterogeneity and tissue distribution of immune cell subsets within the major lineages. Annotation of the T cell **(A,B)**, NK\ILC **(C,D),** B cell (**E,F**), and myeloid cell (**G,H**) subsets was done using MMoCHi. (**A, C, E, G)** The annotated populations for each lineage are projected onto the UMAPs (left) and colored by tissue (right). (**B, D, G, H)** Next to each UMAP embedding is the protein (red matrix plot) and genes (blue dotplot) expression heatmap used to define each population and their relative distribution in each tissue (green heatmap; each row sums to 100%) calculated after downsampling to 79,666 cells (number of cells in the least abundant tissue - ILN) to adjust for the variability in cell number (see Abbreviations section for definitions of cell type labels and tissue labels). **(I)** Immune cell composition by tissue. The cell type composition is displayed as a violin plot where each dot is the frequency of a subset within each donor (frequencies sum to 100% for each donor). Abbreviations: BLD, blood; BMA, bone marrow; SPL, spleen; LN, lymph node: LNG, lung and bronchial alveolar lavage; JEJ, jejunum.

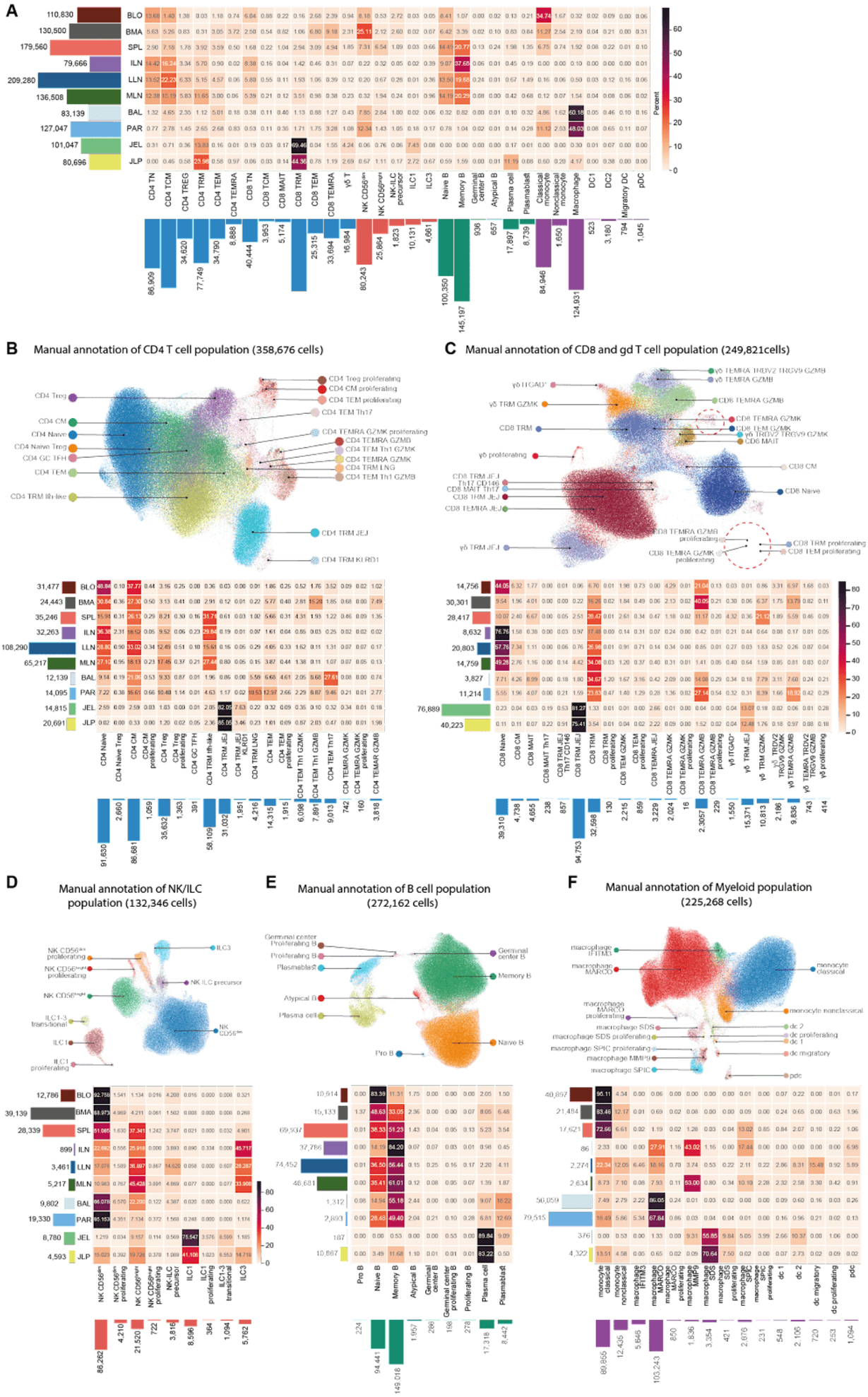

Extended data Figure 2: Tissue distribution and refinement of the MMoCHi annotation identifies additional immune populations. **(A)** Heatmap showing the distribution of each MMoCHi classified immune population per tissue (each row sums to 100%), with barplots on the X and Y axis displaying the total number of cells per cell type and tissue, respectively. Manual annotation was

performed on each of the MMoCHi classified immune populations and for the **(B)** $CD4^+$, **(C)** $CD8^+$, **(D)** NK/ILC, **(E)** B cell and **(F)** Myeloid populations the UMAP is colored by annotation label as well as the frequency of each population per tissue within each immune compartment.

Tissue is a major determinant of immune cell identity and function

To understand how tissue localization influences the transcriptional state of immune cells, we used MrVI to calculate similarity between the ten tissue sites for each of the major immune cell lineages. Hierarchical clustering of the average MrVI distances across lineages revealed high levels of transcriptional similarity within three tissue groups: jejunum (JEL, JLP), lymph nodes (MLN, ILN, LLN) and lung (BAL, PAR), while the remaining sites (blood, BMA, SPL) clustered separately (**Extended data Fig. 3A**). We then performed differential expression (DE) analysis, separately for every major lineage ($CD8^+$ T, $CD4^+$ T, Myeloid, NK/ILC and B cells), comparing each tissue group against the remaining five tissue groups using a pseudo-bulk linear mixed model approach that accounts for the major nuisance covariates in our data (e.g., donor ID, sex, donation site, CMV status)(**Supplementary Table 5**) [31]. The sets of genes from each tissue group that were significantly DE in three or more of the major immune lineages were then merged and hierarchically clustered, resulting in ten gene expression groups and five lineage-tissue groups (**Fig. 3A**). This approach revealed how functional gene profiles are distributed across lineages and tissues.

Certain functional profiles were enriched in specific cell lineages and found across multiple tissue sites (**Fig. 3A**); for example, myeloid cells exhibited specific cell migration and differentiation profiles across all tissues (cluster #4, 5). Other clusters were shared across distinct lineages such as the antigen presentation and costimulatory programs (cluster #3) shared between B and myeloid cells in blood, lymphoid organs, and lung, but lowly expressed the B cells of the jejunum. Another example is the chemokine and cell adhesion cluster (cluster #6) shared between innate lymphocytes, myeloid cells and to a lesser extent $CD8^+$ T cells (**Fig. 3A**). Furthermore, a cluster of genes associated with stem cell-like features (*ITGA6, LEF1, TCF7*) and lymphoid trafficking (*SELL, CCR7*) was enriched within T cells in the blood and LN, and a subset of the genes defining this signature was enriched in B cells in blood, lymphoid organs, and lungs(Cluster #1). Conversely, genes associated with effector function (*IFNG, TBX21, FCGR3A*), and cytotoxicity (*GZMB, GZMK, PRF1, GNLY*) (Cluster #7) were shared between $CD8^+$ T cells, NK/ILC across all tissues except the jejunum, and a subset of genes within this cluster were present in $CD4^+$ T cells in the BMA, spleen, and lungs. Finally, there were several gene expression clusters markedly enriched in NK/ILC and T cells in the jejunum, including genes associated with tissue residence (*ITGAE*, *SPRY1*, *CD248*) (Cluster #9), TRM differentiation (*PRDM1*, *RUNX3*)[32,33], tissue repair (*AREG*)[34], and control of apoptosis and signaling (*BCL2L1*, *PTPN22*) (Cluster #8, 10) (**Fig. 3A)**.

To further investigate these functional signatures across lineages and tissues, we performed differential expression on the surface protein data between tissue sites for each individual donor (**Supplementary Table 6**). Protein abundances were then hierarchically clustered into six major groups, revealing functional signatures similar to the gene expression analysis. Proteins associated with migration and phagocytosis (CD11b, CD11c, CD36; cluster #5) were expressed by myeloid cells in all tissues. Furthermore, proteins associated with antigen presentation (e.g. HLA-DR, CD40, CD1d; cluster #6) were shared between myeloid and B cells in lymphoid sites and the lungs, but less so in the gut B cells (**Fig. 3B**, Clusters #5, 6). We also found a stem-like, lymphoid homing cluster which included expression of CD62L, along with integrins CD49f, CD18, and CD11a by T and NK cells in blood, lungs, and lymphoid organs (**Fig. 3B**, Cluster #1). The effector and cytotoxic cluster (#4) expressing CD16, KLRG1, CD244, GPR56, and CD94 was identified in $CD8^+$ T cells and NK/ILC from multiple sites. Finally, molecules associated with tissue residence including CD103, CD49a, CD101, integrin β7, and CD69 were expressed by T and NK/ILCs, and were highly enriched in the jejunum (**Fig. 3B**, Cluster #3). Together our differential expression analysis validated and extended key signature for immune cell functional states across lineages and tissues.

To specifically interrogate the overall role of tissue in immune cell profiles compared to the more readily profiled and accessible blood, we performed compositional and differential expression analysis of each major lineage in blood versus each tissue. We identified compositional differences between the blood and each tissue site as well as differentially expressed genes across multiple sites for each lineage (**Extended data Fig. 3B-C, Supplementary Fig. 6H**). We found that localization in tissues is accompanied by broad changes in expression of genes associated with metabolism, DNA repair, antigen presentation, cell migration, and post-translational protein modifications. These results suggest that tissue localization may have generalized effects on immune cell functions which are further modified and honed for residence in specific sites, and thus obscured in studies of PBMCs.

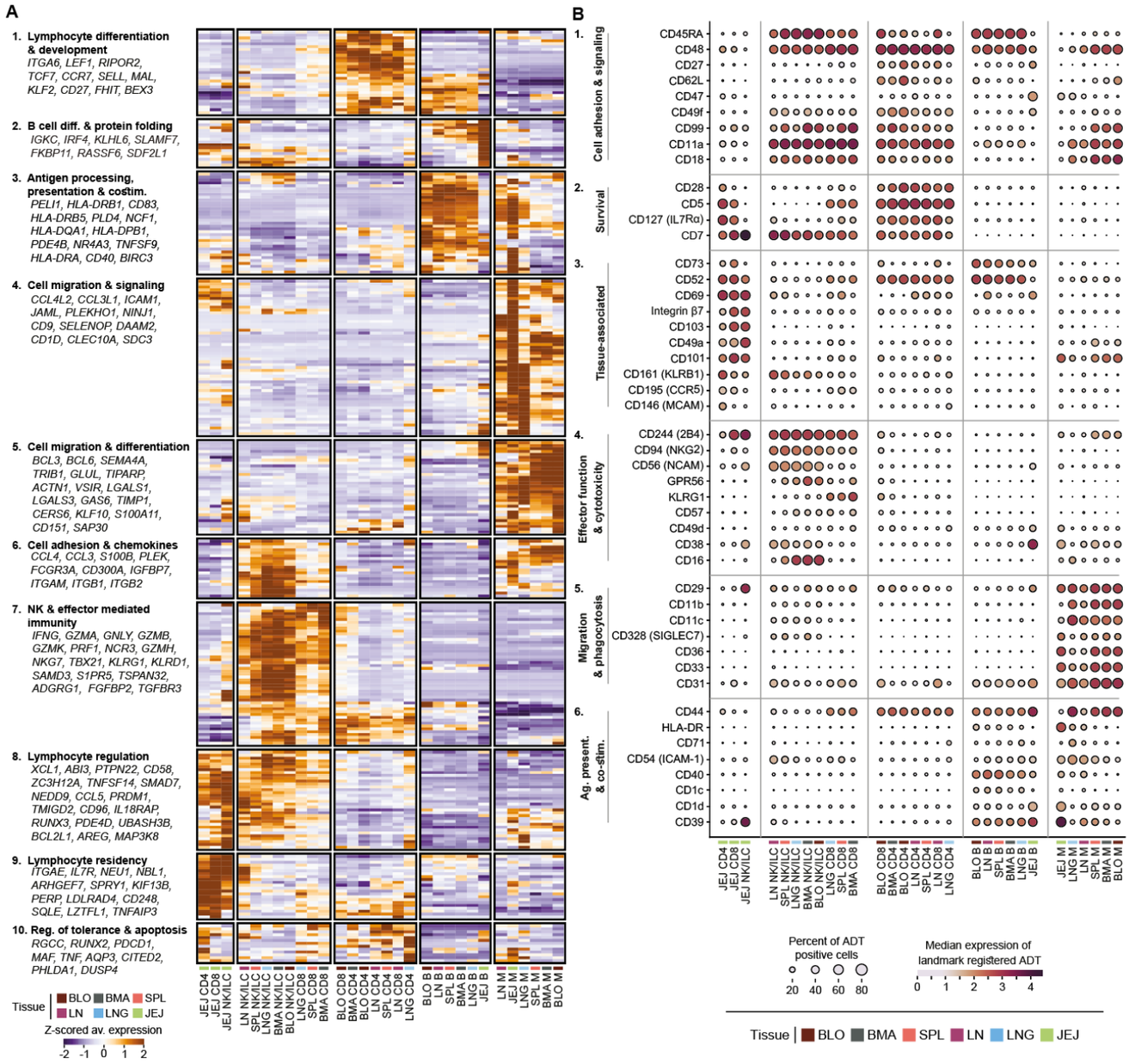

Figure 3: Tissue is a major determinant for immune cell composition and identity. **(A)** Heatmap depicting the expression (Z-score of average expression across cells) of tissue-associated genes. Included are genes that were detected (adj. p-value<0.05, LFC>1) in at least three lineages in at least one of the tissue groups (compared to all other tissue groups). **(B)** Dot plot of significant DE proteins (adj. p-value<0.05, LFC>0.585). Included are proteins that were detected as DE in at least two lineages in at least one of the tissue groups. As the protein DE analysis is conducted separately for each donor, we also require the displayed DE results to hold in at least 65% of donors.

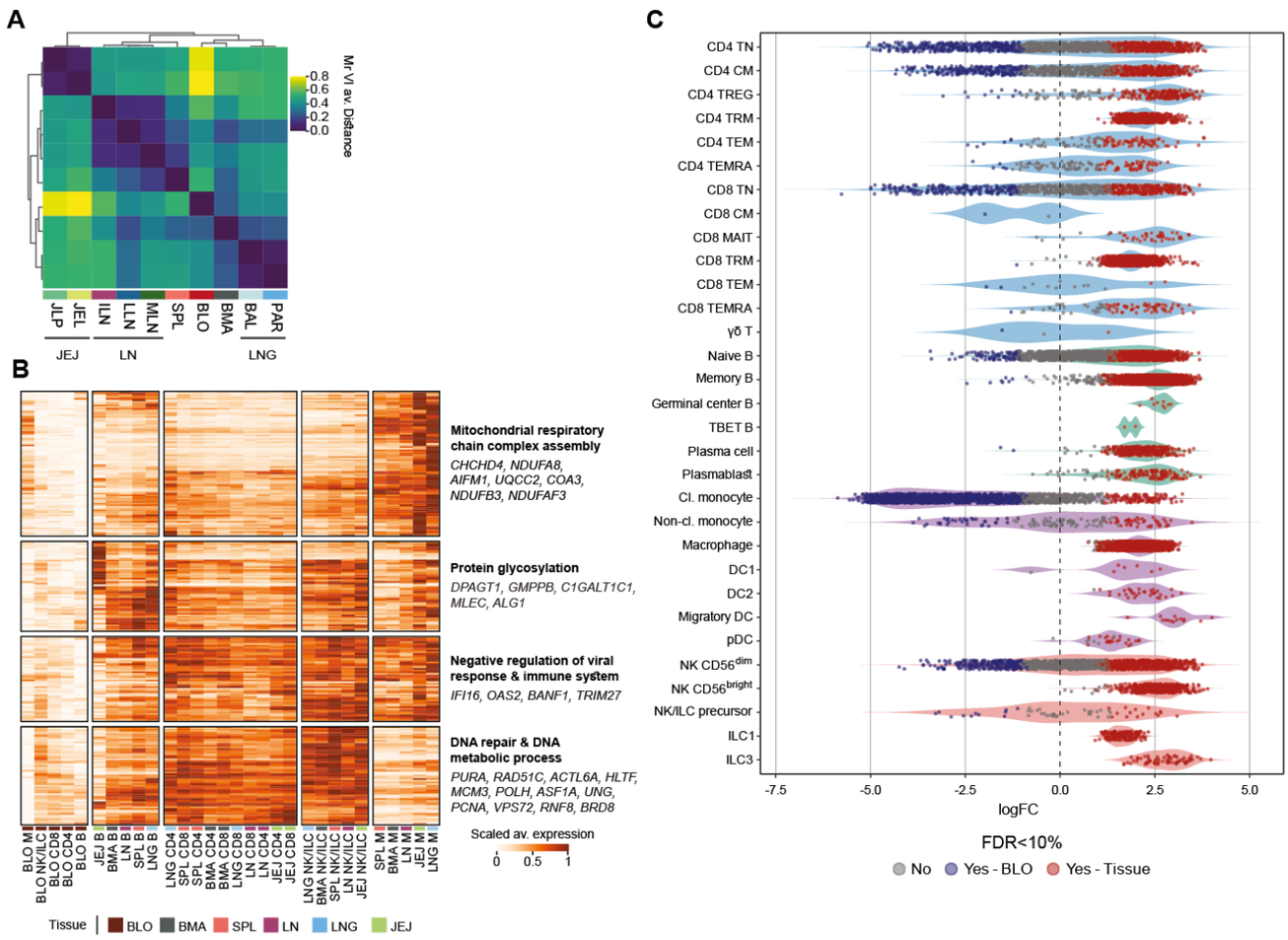

Extended data Figure 3: (A) Heatmap of distances between tissues. Presented are the average distances, across all immune lineages, as evaluated by MrVI. **(B)** Blood vs. tissue comparative analysis. Analysis was conducted separately for each combination of cell lineage and tissue group. Heatmap displayed normalized expression of genes that were DE (adj. p-value<0.05) with positive LFC in at least 80% of the lineage-tissue combinations. **(C)** Violin plot showing neighborhood differential abundance analysis performed with Milo of blood vs. tissue subsets, which highlights tissue enrichment of specific immune populations.

Tissue-specific transcriptional programs across immune lineages

In order to assess whether the tissue imparted distinct gene signatures across lineages, we implemented consensus single cell hierarchical Poisson Factorization (scHPF)[11,35], a Bayesian factorization algorithm that identifies the major co-expression patterns ("factors") in the data, rather than considering each gene in isolation (as we have done for DE). We applied scHPF to each major immune cell lineage in separate models with balanced cell input across tissues (**Supplementary Table 7**), which allowed us to identify a variety of transcriptional programs. We next identified which of the factors were enriched in individual tissues, and hierarchically clustered these factors to reveal distinct groups of gene expression programs or "modules" that were strongly associated with one or more tissues, many of which spanned multiple cell lineages (**Fig. 4A).**

This factorization approach identified three tissue-specific gene expression modules that were manifested across lineages and subsets (**Figs. 4B-J**). Furthermore, as we show by examining module expression within

291 finer-grained immune cell subsets between tissue types by differential expression (**Supplementary Table 8**),
292 these tissue-specific modules are independent of subset composition. The lymphoid module included genes
293 associated with quiescence (*KLF2*, *LEF1, KLF7*) and lymphoid homing (*CCR7*, *SELL, ITGA6*) [36,37], which were
294 enriched in T, B and NK/ILC in LNs and not present in mucosal sites (**Fig. 4B, C**). Importantly, multiple
295 subsets of T cells, including $CD4^+$TCM, $CD4^+$Treg, $CD4^+$TRM, and $CD8^+$TRM, all showed significantly
296 increased expression of lymphoid module genes in the LN compared to mucosal sites (**Fig. 4D**). Second, a
297 "cytotoxicity module" which consisted of multiple effector- and cytotoxicity-associated genes (*GZMH,*
298 *EOMES, NKG7, FGFBP2, ADGRG1*(GPR56), *FCGR3A*), was highly expressed by T cells, NK cells and ILCs
299 in the lung compared to LN and gut, and also enriched in blood, bone marrow and spleen (**Fig. 4A,E, F**).
300 Moreover, $CD8^+$TRM, $CD8^+$TEMRA, γδ T cells and $CD56^{bright}$ NK cells all showed significant enrichment of
301 the cytotoxicity module genes in the lungs when compared to their counterparts in the gut (**Fig. 4G**), further
302 validating the identification of a tissue-driven gene expression program. Lastly, a gut residency module
303 contained genes specific to the jejunum and associated with tissue residency (*CCR9*, *ITGAE*, *CD101*,
304 *CD160*)[12,38] for $CD4^+$ and $CD8^+$ T cells, NK cells and ILCs, while absent in other sites (**Fig. 4H,I**). This module
305 also showed increased expression in $CD4^+$TRM, $CD8^+$TRM, γδ T cells and $CD56^{bright}$ NK cells in the jejunum
306 compared to the lung and LN (**Fig. 4J**). Taken together, these analyses establish that tissue has major effects not
307 only on immune cell composition, but also immune cell transcriptional programs.

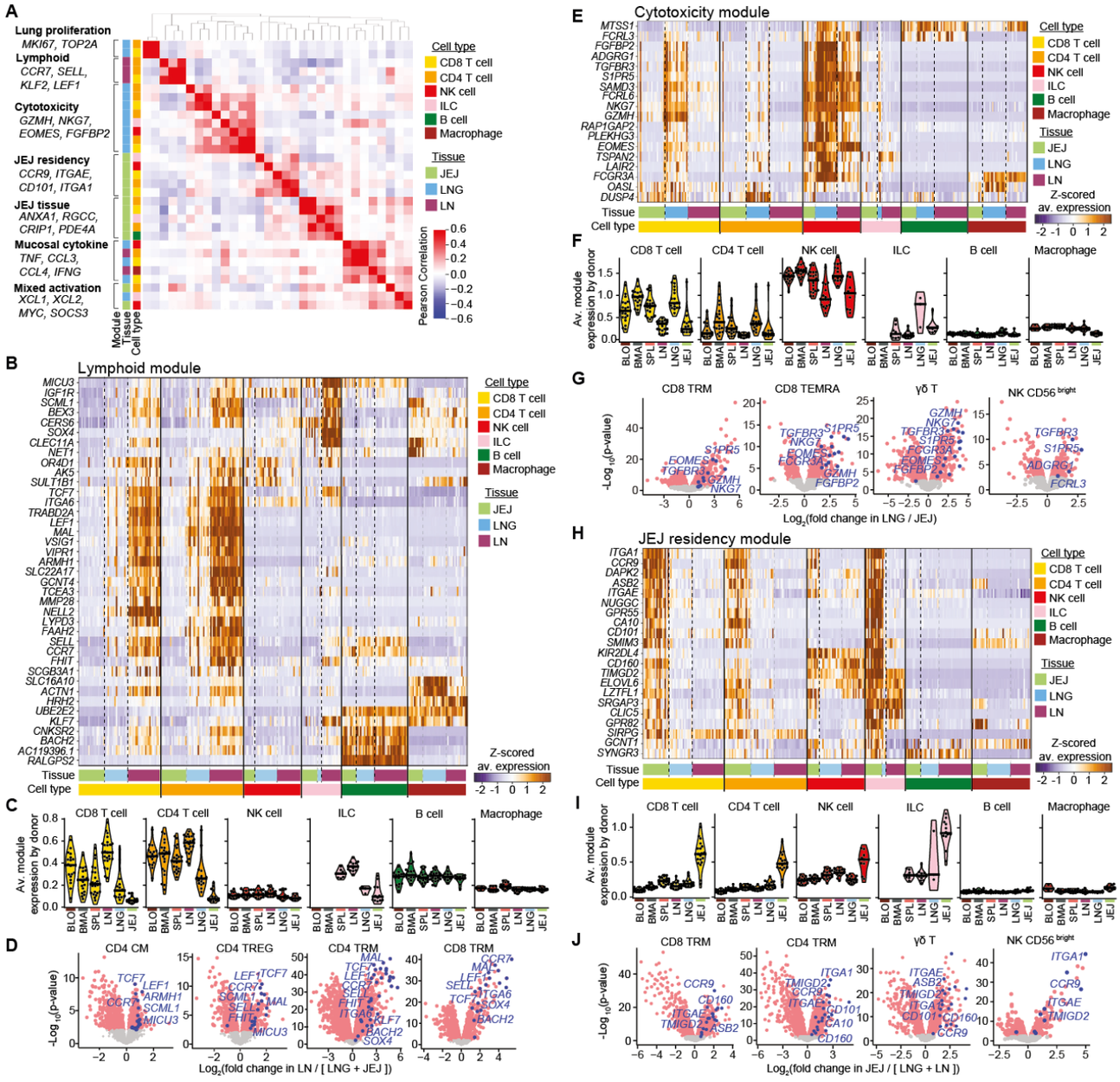

Figure 4: Co-expression programs across immune subsets in tissues. Consensus scHPF was used to factorize gene expression profiles of six immune lineages across three tissues to generate a list of tissue-specific factors. **(A)** Correlogram showing hierarchically-clustered Pearson correlation values between factor gene scores. Seven gene expression modules containing multiple factors with similar transcriptional signatures were identified. The cell type model and tissue enrichment for each of the factors within modules are indicated, with selected top genes within each module listed on the right. **(B)** Heatmap showing z-scored average expression of genes within the Lymphoid module across immune cell subsets and tissues used by scHPF. **(C)** Violin plots showing averaged expression of Lymphoid module genes within a donor across immune cell subset and expanded tissue groupings. **(D)** Volcano plots showing differential expressed transcripts (pink) within selected immune cell subsets across indicated tissues. Genes from the Lymphoid module are indicated in blue. **(E), (F), (G)** Same as **(B), (C)** and **(D)**, but for genes in the Cytotoxicity module. **(H),(I), (J)**, Same as **(B), (C)** and **(D)**, but for genes in the Residency module.

Immune cell aging signatures manifested by specific lineages, subsets, and sites

The age range of the donors spanning six decades of adult life (20–75 years) enabled investigation of age-associated effects across immune lineages and anatomic sites. A global (pseudo-bulk) analysis of variation reveals that while the tissue environment is the dominant factor in the molecular profiles across lineages, aging still explains a fraction of the variance, with some of the most affected genes representing key pathways of immune activation and migration (**Extended data Fig. 5A**). Overall, immune cell composition within each site was maintained over adult age; however, there were decreased frequencies of naïve $CD8^+$ T cells and a decline in subpopulations within naïve B cells, and plasmablasts with age, mostly manifested in blood and LNs (**Extended data Fig. 5B, Supplementary Fig. 7**).

To identify specific gene expression programs that change with age within and across tissues, we applied two complementary approaches. First, we performed a covariate-corrected DE analysis separately for each major immune lineage across tissue groupings and relied on both discrete – comparing pseudo-bulk profiles in younger (< 40 years) versus older (> 40 years) individuals – and continuous tests – single-cell level, considering all ages (**Supplementary Tables 9**, **10**, and **Supplementary Fig. 8**). Second, we generated scHPF models separately for each major lineage with balanced representation for each donor (**Supplementary Table 11**), regressing out covariates to identify expression programs that change with age – comparing normalized scHPF factor scores in younger versus older individuals. Our analysis revealed different classes of genes that are associated with age, including those associated with specific lineages, those associated with specific sites, and a "global aging signature" found across many lineages and sites (**Fig. 5**).

Among myeloid cells, genes encoding pro-inflammatory cytokines, chemokines, and interferon-regulated genes were increased with age in the lung (e.g., *IFIT1/27/44L*, *IL18BP*, *CCRL2*, and *CCL3L1*) and blood (*CXCL16*, *S100A11*, *SLC11A1*) (**Fig. 5A**, cluster #1) . This age-associated increase in pro-inflammatory genes was also observed in classical monocytes from the blood (*CXCL16*, *IFNGR1*, *IRAK1*, *TNFRSF1B*) (**Fig. 5B)**, and in monocytes and macrophages from the lung (*IFIT3/44L*, *IL18BP, MARCO, IL1RN,* **Supplementary Fig. 9A-B**). Conversely, lung macrophages exhibited an age-related decrease in expression of genes encoding apolipoproteins (*APOC1*, *APOC2* and *APOE*), and *TREM2* – a triggering receptor expressed on myeloid cells [39] that binds the lipid binding protein, ApoE, and facilitates macrophage functions, such as phagocytosis and chemotaxis, and induces metabolic changes [40] (**Fig. 5A,C,D**). This *APOE-TREM2* containing module was also identified by scHPF analysis as being decreased in older compared

348 to younger individuals (using the same age cutoff) within myeloid cells in blood-rich tissues (BMA, spleen,
349 blood), LNs, and lungs, but not in the gut (**Fig. 5C**). We validated the age-associated decrease in expression of
350 the *APOE-TREM2* gene module in an independent dataset from human lungs [41] **(Extended data Fig 5C**). While
351 extensive studies have revealed a significant association of *APOE-TREM2* expression in microglia with
352 neurodegeneration in Alzheimer's disease and with macrophages in cardiometabolic disorders in mice and
353 humans [40,42,43], the decreased expression with age in mucosal and lymphoid sites identified here, appears to to be
354 a normal feature of aging.

355 For B cells, there were age-associated increases in expression of genes associated with T-B cell interactions,
356 especially in the spleen and bone marrow, including *CD70* (encoding the ligand for CD27 expressed by memory
357 B cells), *MS4A1* (CD20) and *CLECL1* [44], along with decreased expression of genes involved in cell cycle
358 control (*CDC20, MYBL2*) (**Fig. 5A**, cluster #2). We further identified by scHPF an age-associated decrease in
359 the expression of a gene module associated with RAS signaling (*RASA4B*, *RASGRF1*, *PLAAT3*, *GAB2*) across
360 multiple sites and subsets (**Fig. 5E**). To test the reproducibility of this result, we confirmed that the expression
361 of RAS genes is enriched in bone marrow-derived B cells from younger compared to older donors in an
362 independent dataset[45] (**Extended Data Fig. 5C**). The RAS pathway is coupled to B cell receptor-mediated
363 signaling [46] and has specific roles in memory B cell activation, differentiation and class switching [47]. We also
364 found an age-associated increase in *CD99* within lymph node memory B cells (**Supplementary Table 10**), a
365 surface molecule which signals through the RAS pathway and regulates cell adhesion, survival, and immune
366 cell interactions [48]. Our results therefore suggest alterations in memory B cell signaling and differentiation with
367 age.

368 Among T and NK cells, our analysis identified several aging programs, using DE and scHPF, which are
369 primarily associated with pro-inflammatory and cytotoxic function. One gene module we identified, comprised
370 of multiple pro-inflammatory cytokines and chemokines (e.g., *CCL3*, *CCL4*, *XCL1*, *CXCL2*, *IFNG*, *TNF*) and
371 was increased with age in multiple $CD8^+$ subsets, most prominently TRM, across all tissues (**Fig. 5A**, **F**). A
372 second gene module consisting of cytotoxicity-associated genes (*KLRC3*, *KLRD1*, *KLRF1*, and *GZMB*)
373 increased with age, predominantly in NK at lung and blood-rich sites (**Fig. 5A,** cluster #4, **Supplementary Fig.**
374 **9A**). Finally, scHPF analysis identified an age-associated increase in a gene expression program containing
375 cytotoxicity and activation-associated genes (*GZMK*, *EOMES*, *PDCD1*, *HLA-DR*) manifested by γδ T cells in

all sites and CD8$^+$TEMRA in all sites except the gut (**Fig 5H**). Compositional analysis confirms that there is an increased frequency of *GZMK*-expressing CD8$^+$TEMRA cells in older donors (**Extended Data Fig 5D**), consistent with results in aged mice [49]. By continuous analysis specific to CD8$^+$TEMRA in BMA we further observe increased expression of *GZMK* along with multiple pro-inflammatory chemokines, additional cytotoxicity genes (*KIR3DL2*, *KIR2DL3*) and activation markers (*CD69*, *HLA-DR*, *TIGIT*) (**Fig. 5G**). Finally, TCR analysis shows that these *GZMK*$^+$CD8$^+$TEMRA exhibited increased clonal expansion in older donors (**Extended data Fig. 5E**). Taken together, these results suggest gradual alteration in the activation and effector function of the TEMRA population with age.

The differential expression analysis identified a cluster of genes that exhibited age-related changes across most lineages (**Fig. 5A**, cluster #6). This putative global immune aging signature included increased expression of genes associated with IFN signaling (*IFITM1*, *IFIT2*), mTOR pathways, (*GLA*, *FADS2*, *SLC1A4*, and *RHEBL1* [50]), and pro-inflammatory responses (*PTGER2*, *IRAK2*, *RTP4*, and *TNFSF9*), as well as a marked decrease in expression of multiple genes related to mitochondrial metabolism (*GATD3A*, *AGPAT5*, and *MTRNR2L12)* [51]. These global changes across lineages and tissues are consistent with increased inflammation or “inflammaging” being a major part of the aging process resulting in altered metabolism, increased disease susceptibility, and organ damage [52].

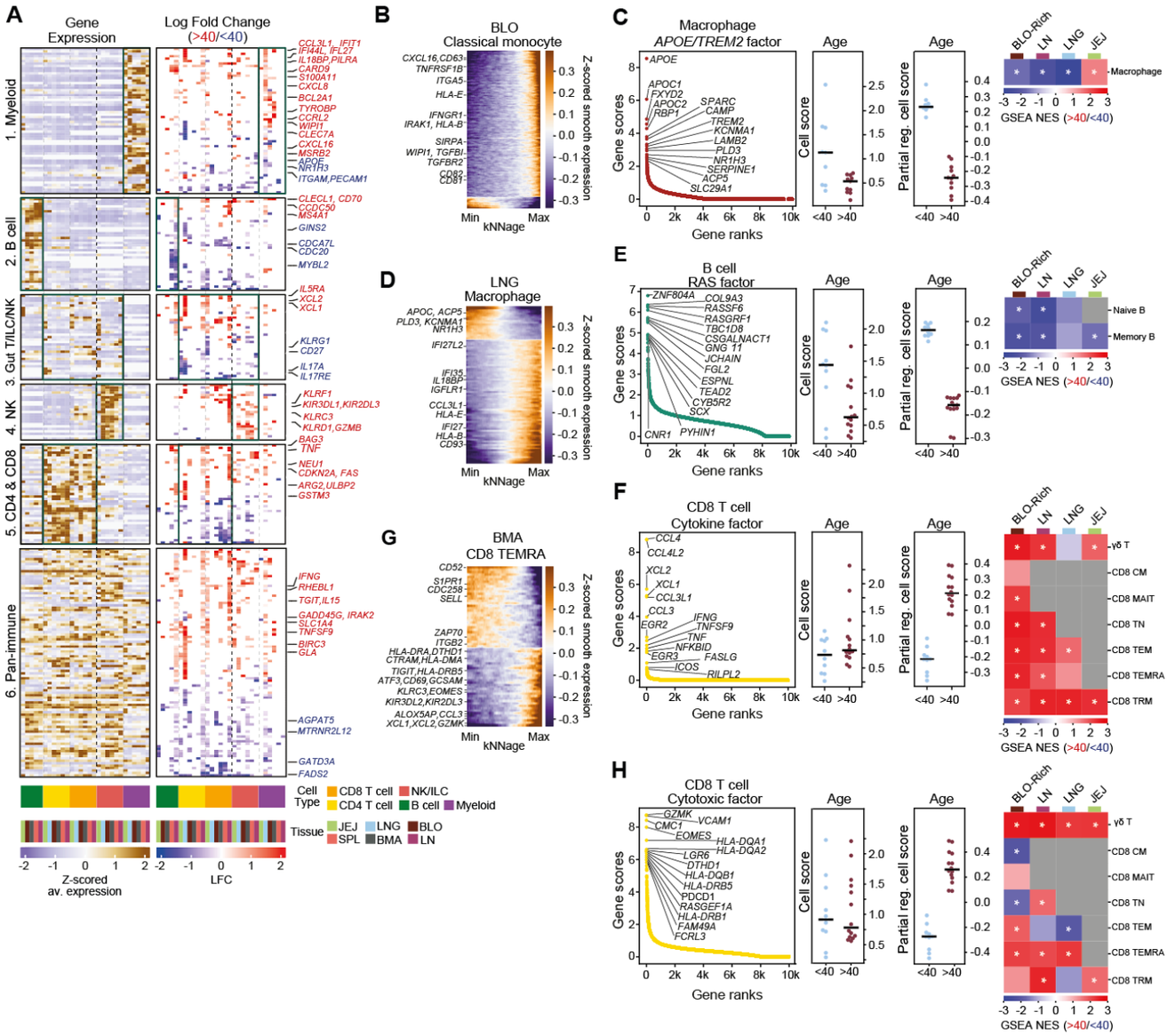

Figure 5: Aging signatures across immune subsets and tissue locations. **(A)** Heatmap depicting age-dependent genes across at least two lineages or two tissues. Clustering by mean expression levels in each combination of tissue-cell lineage (left panel) revealed six groups, highlighting up-regulated (blue) or downregulated (red) genes associated with age (right panel). Fold changes are only displayed for tissue-cell lineage combinations in which the respective gene is expressed at sufficient levels (see Methods) and significantly changes with age (adj p<0.05, |LFC|>0.1). Black lines indicate the most relevant (highest expression) combination of tissue and cell lineage in each gene group. **(B)** kNNage analysis toidentify age-dependent genes in blood monocytes. For this analysis we first assigned each cell with a smooth age coefficient by averaging the donor ages of its 50 nearest neighbors in mrVI latent space. Expression of genes that significantly correlated with these age coefficients (empirical p<0.1, |R|>0.1) is displayed with cells ordered by their age coefficients. Displayed values are Z-scored and smoothed with a sliding window of 5% of cells. **(C)** Dot plot indicating rank and gene scores for the top genes in the *APOE/TREM2* factor derived from the consensus scHPF macrophage model is shown on the left. Factor cell scores and partially regressed cell scores by donor age group are shown in the middle. Heatmap of normalized enrichment scores (NES) by pre-ranked GSEA in the discrete differential expression analysis by cell subset using top 100 ranked genes in the factor as the gene set. **(D)** Same as **(B)** but for macrophages from the lung. **(E)** Same as **(C)** but for the B cell *RAS* Factor identified by consensus scHPF. **(F)** Same as**(C)** but for the CD8$^+$ T cell Cytokine Factor identified by consensus scHPF. **(G)** Same as **(B)** but for CD8$^+$ TEMRA from bone marrow tissues. **(H)** Same as **(C)** but for the CD8$^+$ T cell Cytotoxic Factor identified by consensus scHPF.

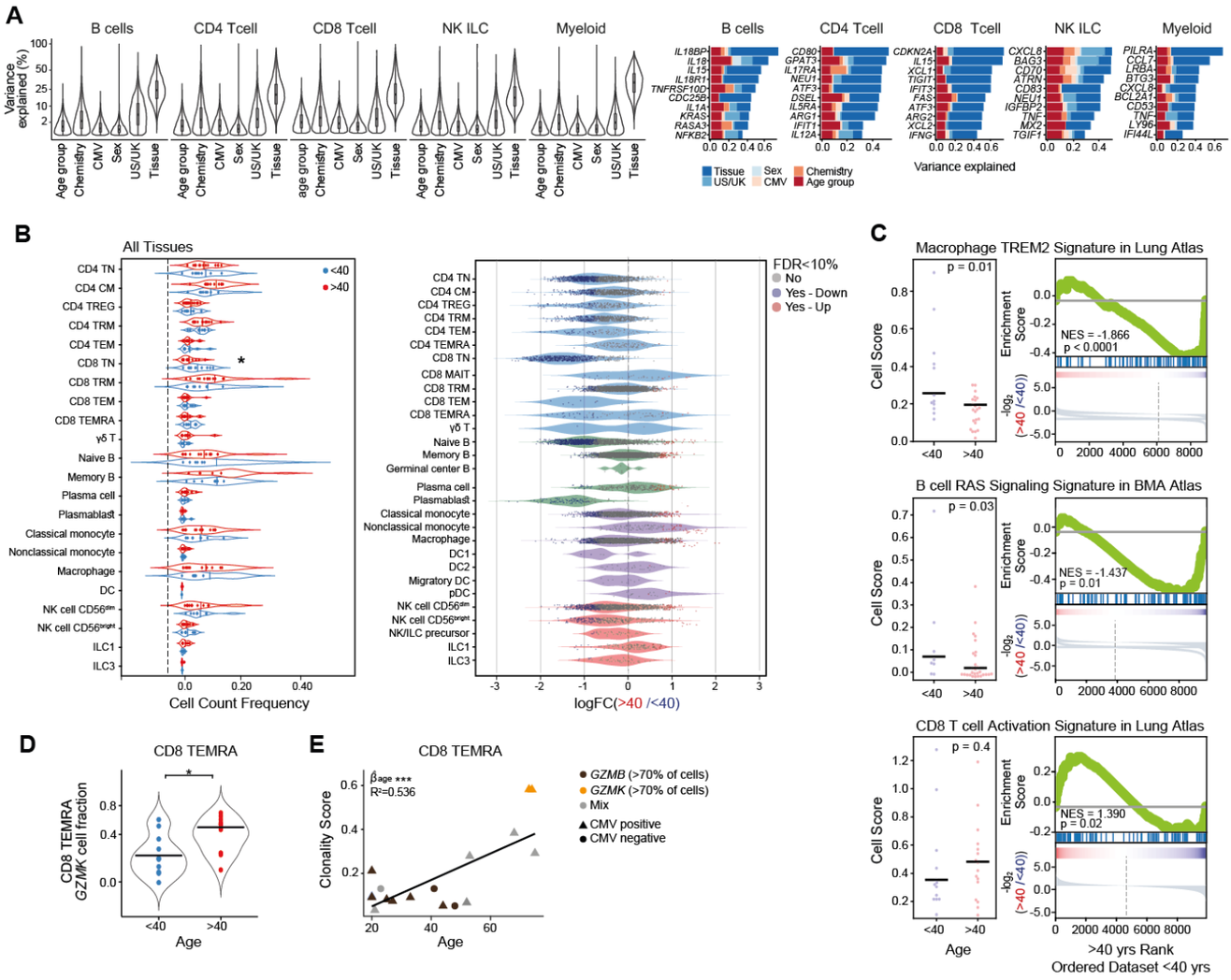

Extended data Figure 5. **(A)** Violin plot summarizing variance partitioning analysis, within each immune lineage, separating the fraction of expression variation for each gene into six components including tissue, age group (over vs. under 40 years old), 10x Genomics chemistry (3' vs. 5'), sex, site of experiment (UK vs. US), and CMV status (positive vs. negative) (left). The variance distribution across these six components in each lineage is displayed for ten representative genes with a high percentage of explained variance by age group (5-20%) (right). **(B)** Changes in cell type abundance with age across all tissues (comparing over vs. under 40 years old donors). (left) Cell type composition is displayed as a violin plot, where each dot represents the frequency of a cell type within each donor (frequencies sum to 100% for each donor). Presented cell types are sufficiently represented (>100 cells) in at least 5 donors in each age group (<40 in blue, >40 in red). Significant differences between age groups are denoted by asterisks (P-values: * <0.05, Wilcoxon test). (right) Violin plot showing neighborhood differential abundance analysis performed with Milo analysis over all tissues. **(C)** scHPF factor cell scores (left) and GSEA analysis (right) showing statistical enrichment of three age-associated factors (top, middle, bottom) among under vs. over 40 year old donors in external datasets. **(D)** Violin plot for the frequency of $CD8^+$ TEMRA $GZMK^+$ cells out of all $CD8^+$ TEMRA cells in blood-rich tissues (BMA, spleen, and blood). Significant differences between age groups (<40 in blue, >40 in red) are denoted in asterisks (P-values: * <0.05, Wilcoxon test). **(E)** Dot plot indicating the clonality score (1−Pielou's evenness index) of CD8+ TEMRA in blood-rich tissues (each dot represents a donor). The CMV status of the respective donor is indicated by shape, and the fraction of $GZMB^+$ and $GZMK^+$ in each $CD8^+$ TEMRA population is reflected by color. Regression line highlights the positive correlation between age and clonality (R2 = 0.57, p <0.001).

Tissue-specific influence of age on the continuum of T helper cell states

While the above analysis examined the effects of age on annotated cell subsets, it is conceivable that some aging effects may be restricted to parts of an annotated subset and/or span several subsets. This is especially the case for T helper ($CD4^+$) cells, which are highly abundant in our data, shared across all tissue sites, and often display a phenotypic continuum rather than separation into well-distinguished subsets [53,54]. For an annotation-independent analysis of aging in $CD4^+$ cells, we leveraged a per-cell estimation of the pertaining effects using counterfactual analysis with MrVI, which considers each cell separately and controls for unwanted covariates (see Methods). This analysis revealed age-related changes for $CD4^+$ T cells in the lung, gut, and lymph nodes that were specific to these sites or manifested differently in other sites (**Fig. 6**) (see complete set of results, for every tissue group and subset in **Extended Report 1**).

In the lung, we detected an age-related gene expression signature in $CD4^+$ TEMRA cells marked by increased expression of certain cytolytic/effector-associated genes (*GZMK, IFNGR1, IL-18R*) concomitant with decreased expression of other genes associated with cytolytic effector function (*PRF1*, *TBX21*) and inflammatory chemokines (*CCL3*, *CCL4L2*)[55,56] **(Fig. 6A-D)**. This pattern of age-related gene expression changes was distinct from $CD8^+$TEMRA, in which age-associated increases in all of these effector-related genes was observed (**Fig. 5G-H**). We trained a classifier to identify similar sets of module-positive cells in each of the other tissues and compared the aging effects on these matched sets to those observed in the lung (Methods). We find that the upregulated effector genes in lung $CD4^+$TEMRA were also upregulated with age in the corresponding populations in all other sites (e.g., blood, BMA, spleen, LN), while the downregulated genes were similarly observed in BMA but exhibited increased expression with age in the blood, spleen and LN **(Fig. 6D)**. Notably, these discordant genes are enriched in cytotoxic effector molecules, such as *PRF1*, *FGFBP2*, and *GZMH*. These results therefore point to age-associated changes in the regulation of cytotoxicity in a major subset of the $CD4^+$ memory pool that is discordant between different tissue sites.

In the jejunum, where the majority of $CD4^+$ T cells are TRM, this analysis highlights a subpopulation of cells with an age-related decline in genes involved in the Th17 pathway including *IL17A*, *IL17F,* and *IL22* and the associated transcription factor *RORC.* These changes are concomitant with increased expression of genes encoding proinflammatory cytokines (*IFNG*, *CSF1*) and activation of the NF-κβ pathway (*NFKBID*), which promotes inflammatory processes (**Fig. 6E-H**). The reduction in IL-17-associated genes coupled with increased

454 *IFNG* has been associated with barrier dysfunction in the gut [55], suggesting a similar effect with aging. Because
455 this CD4$^+$TRM population is specific to the jejunum in our dataset, we investigated potential age-associated
456 changes in CD4$^+$*IL17A*$^+$ cells across all sites where they are found at sufficient numbers in our datasets (i.e.,
457 blood, lung, and LN). This analysis revealed a similar age-associated decline in IL-17-associated genes
458 coincident with an increase in proinflammatory cytokines (e.g., *CSF1*, *CCL20*) in all sites (**Fig. 6H**), suggesting
459 a systemic loss of the Th17 signature with age.

460 A third major age-associated change for CD4$^+$ T cells was found in LN, manifested by the loss of genes
461 which define the T-follicular helper (Tfh) subset[57] including *PDCD1* (encoding PD-1) and *ICA1* along with
462 reduced expression of the stem-like factors *LEF1* and *TCF7*, and an increase in genes associated with T cell
463 activation (*IL2*, *TNFRSF4*, *CD83*) and tissue repair (*AREG*, encoding amphiregulin)[34] (**Fig. 6I-L**). Genes that
464 we found downregulated in the LN show similar trends in the corresponding subpopulations in the lung, BMA,
465 and spleen, while upregulated genes show a similar pattern mostly in the spleen while *AREG* upregulation is
466 specific to LN (**Fig. 6L**). This age-related reduction in Tfh-associated genes across lymphoid sites indicates
467 reduced help for B cell differentiation at the inductive sites for adaptive immunity, potentially accounting for the
468 diminished humoral responses in older age [58,59].

469

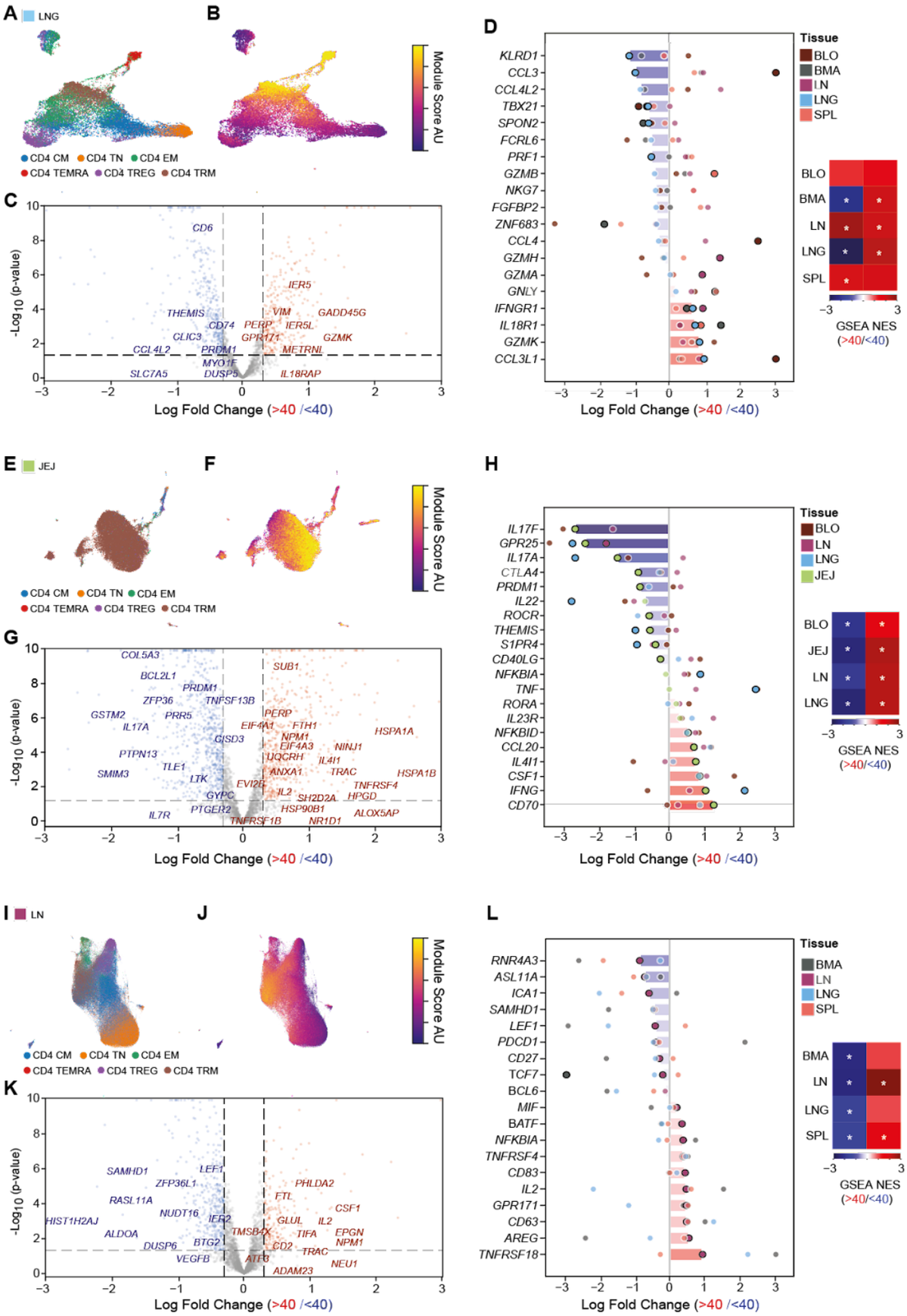

Figure 6. Tissue-dependent signature of aging in CD4$^+$ T cells. MrVI analysis was performed to evaluate age-related effects (LFC) for each gene and in every cell (comparing donors over 40 to under 40 years old). Spectral biclustering of the LFC cell x gene matrix was used to identify gene signatures (i.e., sets of genes with similar aging effects) and the subpopulations of cells in which these effects are manifested (signature-positive cells).**(A)** UMAP embedding of CD4$^+$ T cell-types in the lung. **(B)** UMAP with cells colored by the lung cytotoxicity signature score. Scores are computed by summing the inferred LFCs of signature genes that are upregulated in old individuals minus the sum of LFCs of genes downregulated in old individuals. The respective signature-positive cells are highlighted by high signature scores and overlap with TRM and TEMRA. **(C)** The signature-positive cells were used for pseudo-bulk DE analysis (comparing donors over 40 to under 40 years old) and the top 50 genes from the gene signature (by estimated LFC) are displayed if their unadjusted P-value is below 0.1. **(D)** A classifier was trained to identify signature-positive cells in other tissues. Log-fold changes and p-values were computed using pseudo-bulk DE on these cells (as above). The bars denote the

pseudo-bulk LFC in the lung. All organs are displayed by overlaying circles. Opaque and black circle signifies an unadjusted p-value below 0.05, while transparent and white circle means a p-value above 0.05. We present manually selected genes with known effector or activation functions, which either come from the signature or show similar trend by pseudo-bulk DE in the lung (panel C). GSEA was computed for manually-selected genes to explore their age dependency in other tissues. Separate analysis was conducted to genes that are up or down-regulated in the lung. Gene rankings for GSEA are based on pseudo-bulk DE in the respective tissue. NES scores are displayed and a star means significant with a p-value below 0.1. **(E, F, G,H)** and **(I, J, K, l)** similar to **(A, B,C, D)**. Tissues in **(D, H, I)** are displayed only if a sufficient number of signature-positive cells was detected. Note that differing amounts of signature-positive cells underlies missing significance of genes with high log-fold changes.

DISCUSSION

We present here a comprehensive, high dimensional, global analysis of the human immune system across tissues and ages, through multimodal profiling of blood and tissues from organ donors from the US and UK spanning six decades of adult life. Our findings uncover the basis for the complexity of the immune system and how immune cell identity is shaped by tissue and age. We reveal how tissue imparts key features of immune cell composition, activation, and function and how the immune system alters with age through localized changes to specific immune subsets along with generalized alterations in immune cell capacities. In this way, the immune system provides a highly resilient and adaptive form of protection optimized for the diverse environments of the body and the numerous sources of tissue damage.

The immune system consists of diverse cell lineages and subsets that are found not only in specialized lymphoid organs and blood, but also in diverse mucosal and barrier sites. We show that tissue site is a dominant driver of the immune landscape, determining immune cell composition, cell states, and functional capacity. Of the sites profiled here, intestines had the most distinct immune compartment both in terms of composition and gene expression profiles even compared to lungs, another mucosal/barrier site. In particular, intestinal lymphocytes were mostly TRM (for T cells) and plasma cells (for B cells), and gut-specific gene and protein expression profiles included specific homing receptors, and functions such as IL-17 production. Similarly, LN also exerted specific functional and differentiation properties on immune cells, maintaining them in more quiescent and stem-like states. By contrast, lungs, spleen, BMA and blood contained lymphocyte populations with more pro-inflammatory profiles, but distinct myeloid lineage cells with tissue-specific properties. Between lineages, T, NK/ILC, and myeloid lineage cells exhibited dominant tissue-specific features while B cells did not, indicating that B cell identity is less influenced by location.

The tissue-specific signatures identified here have important relevance for immune monitoring and immunotherapies. The compartmentalization of subsets and functional responses in tissues compared to blood, suggests that monitoring tissue-directed responses is not readily assessed in circulation. Indeed, in studies of

516 responses to respiratory infection with SARS-CoV-2, the lymphocyte and myeloid cell responses in the
517 respiratory tract were distinct from blood and correlated more with infection outcome [60,61]. In addition, the
518 striking segregation of gut-specific subsets and profiles indicates that oral administration of vaccines would be
519 optimal for promoting protection to intestinal pathogens, as demonstrated for the success of rotavirus vaccines
520 [62]. Another clinically relevant finding in our tissue data includes the identification of stem-like profiles for T and
521 NK cells in lymph nodes. As expression of *TCF7* and *LEF1* is associated with complete and partial remission in
522 CAR-T immunotherapies [63], the isolation of NK and T cells from LN may constitute optimal sources for
523 generating CAR-T for anti-tumor and anti-viral therapies.

524 Our dataset enabled a novel assessment of how immune cells across the body become altered with age. We
525 found that age-associated changes were for the most part, specific to lineage and site. For macrophages in lungs
526 and lymphoid organs (but not gut), we found a reduction of the *APOE-TREM2* axis with age. TREM2 can have
527 different effects on macrophage function, depending on context; it has been associated with induction of
528 anti-inflammatory M2 function during infection, but can also promote phagocytosis and sustained inflammation
529 in other infectious conditions [64,65]. Notably, TREM2 expression in microglia has been widely associated with
530 age-driven dementia in Alzheimer's disease, and more recently, TREM2-macrophages have been associated
531 with immunosuppression and lack of responses to immunotherapy in tumors [66]. The loss of TREM2 over age
532 may be due to increased binding by ApoE and could serve as an adaptation to restrict macrophage activation or
533 regulation in tissues. This alteration in regulation of macrophage function with age is important to dissect in
534 future studies to determine whether it plays a role in the increased susceptibility to respiratory pathogens and
535 lung cancer with age.

536 Other age-associated features were specific to lineages in certain sites. T cells and NK cells in circulation
537 were functionally altered with age, expressing higher levels of genes associated with inflammation, cytotoxicity,
538 and migration, reflecting previous findings in blood [67]. By contrast, T cells resident in tissues (such as the gut
539 and lung) were impaired in their ability to produce pro-inflammatory cytokines such as IL-17, which is
540 associated with reduced barrier immunity [68], suggesting compromised *in situ* protection over age. These
541 impaired tissue responses may result in reduced immune surveillance of an organ and predispose for tumor
542 formation with age as observed for lung and colon cancer– diseases of the elderly [69]. The increased systemic
543 inflammation and cytotoxicity of surveilling T and NK populations can have both deleterious effects causing
544 tissue damage, but can also help clear senescent cells [70,71]. Our results also reveal a potential switch to more T

cell proliferation and tissue repair functions with age in LN, possibly in response to age-associated tissue damage.

The immune system is distinct in being distributed throughout the body, in its ability to establish memory as resident populations in diverse anatomic sites, and in its ability to adapt with each pathogen encounter and environmental exposure [8]. In order to meet the complex demands of the host for protection from pathogens and mediators of tissue injury, immune cells require plasticity but also stability, to prevent dysregulated responses that can lead to tissue damage. Through our extensive and deep profiling of immune lineages across organs and tissue systems, we show how immune cell identity is layered, with lineage being the foundation upon which function and fate are determined, followed by location playing major roles in subset delineation and function, with more subtle changes occurring with age. We reveal that lymphocytes undergo distinct age-associated changes depending on the site; there is increased inflammation in circulation while immune potency appears to be better preserved in lymphoid organs. Together, our dataset, models, and analyzes can serve as a comprehensive and actionable resource to inform targeted immune modulation by site and age in future treatments for infectious, neoplastic, and inflammatory diseases.

AUTHOR CONTRIBUTIONS

N.Y., D.L.F., P.A.S., J.J., and S.A.T. designed the study; M.K., R.M., K.M., and K.S.-P. obtained tissues from deceased organ donors; S.B.W., D.B.R., P.A.Sz, D.P.C., S.K.H., L.B.J., L.E., D.C. performed tissue dissociation and prepared single-cell sequencing libraries; M.M., C.E., S.B.W., D.R., P.A.S., P.A.Sz, D.P.C., A.R.M., E.R., V.V.P.A analyzed and interpreted the data; D.L.F., N.Y., P.A.S., J.J. supervised experiments; N.Y. and P.A.S. coordinated data analysis; D.L.F., N.Y., P.A.S., J.J, S.A.T, S.B.W., D.B.R., M.M., P.A.Sz., C.E., A.R.M. wrote and edited the manuscript. N.Y., D.L.F., P.A.S., J.J., S.A.T. provided funding. All authors read, provided input on, and approved the manuscript.

ACKNOWLEDGEMENTS

We thank the deceased organ donors, donor families, the extended Cambridge Biorepository for Translational Medicine (CBTM) team, and the transplant coordinators at LiveOnNY for access to the tissue samples. This work was supported by a Chan-Zuckerberg Initiative Seed Networks for the Human Cell Atlas grant (CZF2019-002452) to N.Y, D.L.F., P.A.S., J.J., and S.T., along with NIH grants AI106697, AI128949 awarded to D.L.F. and P.A.S and NIHR Cambridge Biomedical Research Centre funding to J.J (BRC-1215-20014). D.P.C. was supported by the Columbia University Graduate Training Program in Microbiology and Immunology (T32AI106711). Flow cytometry analysis was performed in the CCTI Flow Cytometry Core supported by NIH S10RR027050 and S10OD020056 and the Cambridge NIHR BRC Cell Phenotyping Hub (Department of Medicine, University of Cambridge). The views expressed here are those of the author(s) and not necessarily those of the NIHR, Department of Health and Social Care, or National Institutes of Health (NIH).

Conflict of Interest

In the past three years JJ has consulted for, or been a member of a scientific advisory board for Sanofi, Roche and Enhanc3DGenomics, and S.A.T. has consulted for or been a member of scientific advisory boards at Qiagen, Sanofi, GlaxoSmithKline, and ForeSite Labs. She is a consultant and equity holder for TransitionBio and EnsoCell.

REFERENCES

1. Szabo, P. A., Miron, M. & Farber, D. L. Location, location, location: Tissue resident memory T cells in mice and humans. *Sci Immunol* **4**, eaas9673. (2019).
2. Terekhova, M. *et al.* Single-cell atlas of healthy human blood unveils age-related loss of NKG2C+GZMB-CD8+ memory T cells and accumulation of type 2 memory T cells. *Immunity* **56**, 2836–2854.e9 (2023).
3. Tabula Sapiens Consortium* *et al.* The Tabula Sapiens: A multiple-organ, single-cell transcriptomic atlas of humans. *Science* **376**, eabl4896 (2022).
4. Sikkema, L. *et al.* An integrated cell atlas of the lung in health and disease. *Nat. Med.* **29**, 1563–1577 (2023).
5. Aizarani, N. *et al.* A human liver cell atlas reveals heterogeneity and epithelial progenitors. *Nature* **572**, 199–204 (2019).
6. Siletti, K. *et al.* Transcriptomic diversity of cell types across the adult human brain. *Science* **382**, eadd7046 (2023).
7. Marečková, M. *et al.* An integrated single-cell reference atlas of the human endometrium. *bioRxiv* 2023.11.03.564728 (2023) doi:10.1101/2023.11.03.564728.
8. Yosef, N. & Regev, A. Writ large: Genomic dissection of the effect of cellular environment on immune response. *Science* **354**, 64–68 (2016).
9. Thome, J. J. *et al.* Spatial map of human T cell compartmentalization and maintenance over decades of life. *Cell* **159**, 814–828 (2014).
10. Miron, M. *et al.* Human Lymph Nodes Maintain TCF-1(hi) Memory T Cells with High Functional Potential and Clonal Diversity throughout Life. *J. Immunol.* **201**, 2132–2140 (2018).
11. Szabo, P. A. *et al.* Single-cell transcriptomics of human T cells reveals tissue and activation signatures in health and disease. *Nat. Commun.* **10**, 4706 (2019).
12. Poon, M. M. L. *et al.* Tissue adaptation and clonal segregation of human memory T cells in barrier sites. *Nat. Immunol.* **24**, 309–319 (2023).
13. Dominguez Conde, C. *et al.* Cross-tissue immune cell analysis reveals tissue-specific features in humans. *Science* **376**, eabl5197 (2022).
14. Kumar, B. V., Connors, T. J. & Farber, D. L. Human T Cell Development, Localization, and Function throughout Life. *Immunity* **In Press**, 202–213 (2018).
15. Dogra, P. *et al.* Tissue Determinants of Human NK Cell Development, Function, and Residence. *Cell* **180**,

749–763 e13 (2020).

16. Kumar, B. V. *et al.* Human Tissue-Resident Memory T Cells Are Defined by Core Transcriptional and Functional Signatures in Lymphoid and Mucosal Sites. *Cell Rep.* **20**, 2921–2934 (2017).

17. Boyeau, P. *et al.* Deep generative modeling for quantifying sample-level heterogeneity in single-cell omics. *bioRxiv* 2022.10.04.510898 (2022) doi:10.1101/2022.10.04.510898.

18. Becht, E. *et al.* Dimensionality reduction for visualizing single-cell data using UMAP. *Nat. Biotechnol.* (2018) doi:10.1038/nbt.4314.

19. Caron, D. P. *et al.* Multimodal hierarchical classification of CITE-seq data delineates immune cell states across lineages and tissues. *bioRxiv* (2023) doi:10.1101/2023.07.06.547944.

20. Sallusto, F., Lenig, D., Forster, R., Lipp, M. & Lanzavecchia, A. Two subsets of memory T lymphocytes with distinct homing potentials and effector functions [see comments]. *Nature* **401**, 708–712 (1999).

21. Zheng, Y. & Rudensky, A. Y. Foxp3 in control of the regulatory T cell lineage. *Nat. Immunol.* **8**, 457–462 (2007).

22. Thome, J. J. *et al.* Early-life compartmentalization of human T cell differentiation and regulatory function in mucosal and lymphoid tissues. *Nat. Med.* **22**, 72–77 (2016).

23. Provine, N. M. & Klenerman, P. MAIT Cells in Health and Disease. *Annu. Rev. Immunol.* **38**, 203–228 (2020).

24. Miron, M. *et al.* Maintenance of the human memory T cell repertoire by subset and tissue site. *Genome Med.* **13**, 100 (2021).

25. Yudanin, N. A. *et al.* Spatial and Temporal Mapping of Human Innate Lymphoid Cells Reveals Elements of Tissue Specificity. *Immunity* **50**, 505–519 e4 (2019).

26. Muramatsu, M. *et al.* Class switch recombination and hypermutation require activation-induced cytidine deaminase (AID), a potential RNA editing enzyme. *Cell* **102**, 553–563 (2000).

27. Sutton, H. J. *et al.* Atypical B cells are part of an alternative lineage of B cells that participates in responses to vaccination and infection in humans. *Cell Rep.* **34**, 108684 (2021).

28. Johnson, J. L. *et al.* The Transcription Factor T-bet Resolves Memory B Cell Subsets with Distinct Tissue Distributions and Antibody Specificities in Mice and Humans. *Immunity* **52**, 842–855 e6 (2020).

29. Weisel, N. M. *et al.* Comprehensive analyses of B-cell compartments across the human body reveal novel subsets and a gut-resident memory phenotype. *Blood* **136**, 2774–2785 (2020).

30. Ergen, C. *et al.* Consensus prediction of cell type labels with popV. *bioRxiv* 2023.08.18.553912 (2023) doi:10.1101/2023.08.18.553912.

31. Hoffman, G. E. *et al.* Efficient differential expression analysis of large-scale single cell transcriptomics data using dreamlet. *bioRxiv* (2023) doi:10.1101/2023.03.17.533005.

32. Mackay, L. K. *et al.* Hobit and Blimp1 instruct a universal transcriptional program of tissue residency in lymphocytes. *Science* **352**, 459–463 (2016).

33. Milner, J. J. *et al.* Heterogenous Populations of Tissue-Resident CD8(+) T Cells Are Generated in Response to Infection and Malignancy. *Immunity* **52**, 808–824 e7 (2020).

34. Zaiss, D. M. W., Gause, W. C., Osborne, L. C. & Artis, D. Emerging functions of amphiregulin in orchestrating immunity, inflammation, and tissue repair. *Immunity* **42**, 216–226 (2015).

35. Levitin, H. M., Zhao, W., Bruce, J. N., Canoll, P. & Sims, P. A. Consensus scHPF Identifies Cell Type-Specific Drug Responses in Glioma by Integrating Large-Scale scRNA-seq. *bioRxiv* (2023) doi:10.1101/2023.12.05.570193.

36. Shan, Q. *et al.* Tcf1 and Lef1 provide constant supervision to mature CD8+ T cell identity and function by organizing genomic architecture. *Nat. Commun.* **12**, 5863 (2021).

37. Schuettpelz, L. G. *et al.* Kruppel-like factor 7 overexpression suppresses hematopoietic stem and progenitor cell function. *Blood* **120**, 2981–2989 (2012).

38. Gray, J. I. & Farber, D. L. Tissue-Resident Immune Cells in Humans. *Annu. Rev. Immunol.* **40**, 195–220 (2022).

39. Lavin, Y. *et al.* Tissue-resident macrophage enhancer landscapes are shaped by the local microenvironment. *Cell* **159**, 1312–1326 (2014).

40. Bohlen, C. J., Friedman, B. A., Dejanovic, B. & Sheng, M. Microglia in Brain Development, Homeostasis, and Neurodegeneration. *Annu. Rev. Genet.* **53**, 263–288 (2019).

41. Natri, H. M. *et al.* Cell type-specific and disease-associated eQTL in the human lung. *bioRxiv* (2023) doi:10.1101/2023.03.17.533161.

42. Krasemann, S. *et al.* The TREM2-APOE Pathway Drives the Transcriptional Phenotype of Dysfunctional Microglia in Neurodegenerative Diseases. *Immunity* **47**, 566–581.e9 (2017).

43. Deczkowska, A., Weiner, A. & Amit, I. The Physiology, Pathology, and Potential Therapeutic Applications of the TREM2 Signaling Pathway. *Cell* **181**, 1207–1217 (2020).

44. Ryan, E. J. *et al.* Dendritic cell-associated lectin-1: a novel dendritic cell-associated, C-type lectin-like molecule enhances T cell secretion of IL-4. *J. Immunol.* **169**, 5638–5648 (2002).

45. Lee, N. Y. S., Li, M., Ang, K. S. & Chen, J. Establishing a human bone marrow single cell reference atlas to study ageing and diseases. *Front. Immunol.* **14**, 1127879 (2023).

46. Oh-hora, M., Johmura, S., Hashimoto, A., Hikida, M. & Kurosaki, T. Requirement for Ras guanine nucleotide releasing protein 3 in coupling phospholipase C-gamma2 to Ras in B cell receptor signaling. *J. Exp. Med.* **198**, 1841–1851 (2003).

47. Takahashi, Y. *et al.* Novel role of the Ras cascade in memory B cell response. *Immunity* **23**, 127–138 (2005).

48. Pasello, M., Manara, M. C. & Scotlandi, K. CD99 at the crossroads of physiology and pathology. *J. Cell Commun. Signal.* **12**, 55–68 (2018).

49. Mogilenko, D. A. *et al.* Comprehensive Profiling of an Aging Immune System Reveals Clonal GZMK(+) CD8(+) T Cells as Conserved Hallmark of Inflammaging. *Immunity* **54**, 99–115 e12 (2021).

50. Xiao, B. *et al.* Rheb1-Independent Activation of mTORC1 in Mammary Tumors Occurs through Activating Mutations in mTOR. *Cell Rep.* **31**, 107571 (2020).

51. McGuire, P. J. Mitochondrial Dysfunction and the Aging Immune System. *Biology* **8**, (2019).

52. Franceschi, C., Garagnani, P., Parini, P., Giuliani, C. & Santoro, A. Inflammaging: a new immune-metabolic viewpoint for age-related diseases. *Nat. Rev. Endocrinol.* **14**, 576–590 (2018).

53. Persad, S. *et al.* SEACells infers transcriptional and epigenomic cellular states from single-cell genomics data. *Nat. Biotechnol.* (2023) doi:10.1038/s41587-023-01716-9.

54. Gaublomme, J. T. *et al.* Single-Cell Genomics Unveils Critical Regulators of Th17 Cell Pathogenicity. *Cell* **163**, 1400–1412 (2015).

55. Cai, Y. *et al.* Single-cell immune profiling reveals functional diversity of T cells in tuberculous pleural effusion. *J. Exp. Med.* **219**, (2022).

56. Oja, A. E. *et al.* Trigger-happy resident memory CD4+ T cells inhabit the human lungs. *Mucosal Immunol.* **11**, 654–667 (2018).

57. Crotty, S. Follicular helper CD4 T cells (TFH). *Annu. Rev. Immunol.* **29**, 621–663 (2011).

58. Collier, D. A. *et al.* Age-related immune response heterogeneity to SARS-CoV-2 vaccine BNT162b2. *Nature* (2021) doi:10.1038/s41586-021-03739-1.

59. Goronzy, J. J. & Weyand, C. M. Understanding immunosenescence to improve responses to vaccines. *Nat. Immunol.* **14**, 428–436 (2013).

60. Zhang, W. *et al.* SARS-CoV-2 infection results in immune responses in the respiratory tract and peripheral blood that suggest mechanisms of disease severity. *Nat. Commun.* **13**, 2774 (2022).

61. Szabo, P. A. *et al.* Longitudinal profiling of respiratory and systemic immune responses reveals myeloid cell-driven lung inflammation in severe COVID-19. *Immunity* **54**, 797–814 e6 (2021).

62. Folorunso, O. S. & Sebolai, O. M. Overview of the Development, Impacts, and Challenges of Live-Attenuated Oral Rotavirus Vaccines. *Vaccines (Basel)* **8**, (2020).

63. Fraietta, J. A. *et al.* Determinants of response and resistance to CD19 chimeric antigen receptor (CAR) T cell therapy of chronic lymphocytic leukemia. *Nat. Med.* **24**, 563–571 (2018).

64. Matos, A. de O., Dantas, P. H. D. S., Queiroz, H. A. G. de B., Silva-Sales, M. & Sales-Campos, H. TREM-2: friend or foe in infectious diseases? *Crit. Rev. Microbiol.* 1–19 (2022).

65. Wu, K. *et al.* TREM-2 promotes macrophage survival and lung disease after respiratory viral infection. *J. Exp. Med.* **212**, 681–697 (2015).

66. Zhang, H. *et al.* Immunosuppressive TREM2(+) macrophages are associated with undesirable prognosis and responses to anti-PD-1 immunotherapy in non-small cell lung cancer. *Cancer Immunol. Immunother.* **71**, 2511–2522 (2022).

67. Pereira, B. I. *et al.* Sestrins induce natural killer function in senescent-like CD8(+) T cells. *Nat. Immunol.* **21**, 684–694 (2020).

68. Merino, K. M., Jazwinski, S. M. & Rout, N. Th17-type immunity and inflammation of aging. *Aging* **13**, 13378–13379 (2021).

69. Foster, A. D., Sivarapatna, A. & Gress, R. E. The aging immune system and its relationship with cancer. *Aging health* **7**, 707–718 (2011).

70. Laphanuwat, P., Gomes, D. C. O. & Akbar, A. N. Senescent T cells: Beneficial and detrimental roles. *Immunol. Rev.* (2023) doi:10.1111/imr.13206.

71. Hasegawa, T. *et al.* Cytotoxic CD4+ T cells eliminate senescent cells by targeting cytomegalovirus antigen. *Cell* **186**, 1417–1431.e20 (2023).